

Transport Theory-Based Multi-Spectral Imaging of Tissue Chromophores Concentrations

Hyun Keol Kim¹, James Masciotti¹, Andreas H. Hielscher^{1,2}

¹Department of biomedical engineering, Columbia University, 351 Engineering Terrace., 500 West 120th St., New York, NY 10027

²Department of Radiology, Columbia University, 660 West 168th St., New York, New York 10327
e-mail address: ahh2004@columbia.edu

Abstract: We introduce a transport-theory-base multi-spectral inverse method for direct recovery of the spatial distributions of chromophores inside biomedical tissues. To illustrate the code's performance, we present numerical studies and first results from experiments on tumor bearing mice. It is shown that the spectrally-constrained direct method produces physically more accurate results than the conventional two-step approach.

©2007 Optical Society of America

OCIS codes: (110.4234) Multispectral and hyperspectral imaging; (170.5280) Photon migration

1. Introduction

Until recently, the most common approach to obtain the tomographic images of chromophore concentrations in tissue was based on a two-step method. In this method, first the absorption coefficients are retrieved for several wavelengths independently. In a second step the information from each wavelength is combined to obtain, for example, the hemoglobin concentrations through a direct matrix inversion or a least-squared method [1]. However, it has been reported that this two-step approach can sometimes produce unphysical results, and often shows strong cross-talk between different chromophores [2]. To overcome this problem, several groups have independently pursued a new approach that directly retrieves chromophore concentrations by forcing spectral consistency into the reconstruction process. Li et al [2] proposed a direct method that is based on perturbation theory, while Corlu et al [3,4] explored wavelength optimization for continuous-wave multi-spectral optical tomography. However, all these studies employed the diffusion theory, which is of limited value in small-animal imaging [5]. This motivates the development of a generalized multi-spectral method that is based on the transport theory, which has been shown to work well in small geometries and other media in which the diffusion approximation is of limited accuracy.

2. Methods: Forward and inverse models with spectral constraints

The frequency domain forward model for light propagation in tissue can be accurately modeled by the radiative transfer equation as [6,7]

$$[\Omega \cdot \nabla + \mu_a^\lambda + \mu_s^\lambda + i\frac{\omega}{c}]I_\lambda(\vec{r}, \Omega, \omega) = \frac{\mu_s^\lambda}{4\pi} \int_{4\pi} I_\lambda(\vec{r}, \Omega^+, \omega) \Phi(\Omega^+, \Omega) d\Omega^+ \quad (1)$$

where I_λ is the spectral radiation intensity in unit [W/cm²/sr/nm], and $\mu_a(\lambda)$ and $\mu_s(\lambda)$ are the wavelength-dependent absorption and scattering coefficient in unit [1/cm], and Φ is the phase function describing scattering from direction Ω^+ into direction Ω . We use here the Henyey-Greenstein phase function that is commonly used in tissue optics. To solve the forward problem for the spectral intensity we have implemented a GMRES solver [8].

If a chromophore concentration is reconstructed, the linear mapping function of the i -th chromophore concentration C_i to the absorption coefficient $\mu_a(\lambda)$ is given with the i -th absorption extinction coefficient $\epsilon_i(\lambda)$ as $\mu_a(\lambda) = \sum [\epsilon_j][C_j]$ where ϵ_j 's denote the molar extinction coefficients of chromophores whose values are available in the literature [9]. In the multi-spectral inverse model, we directly retrieve the spatial distributions of the chromophore concentrations by employing data obtained from measurements at multiple wavelengths simultaneously. Accordingly, the associated inverse problem reduces to minimizing the sum of the objective function defined at each wavelength as:

$$\phi[C_i] = \sum_{n=1}^{N_\lambda} \phi[\mu_a^{\lambda_n}, \mu_s^{\lambda_n}] = \frac{1}{2} \sum_{n=1}^{N_\lambda} \sum_{d=1}^{ND} \|M_d^{\lambda_n} - P_d^{\lambda_n}\| \quad (2)$$

where N_λ is the number of measurement wavelengths and C_i is the i -th chromophore concentration that can be either [HbO₂] or [Hb] or [Water] or [Lipid] concentrations. In a practical reconstruction step, the minimization of the multi-spectral data-based objective function (2) can be realized by incorporating the spectral data into the gradients of the objective function with respect to the chromophore concentrations. Thus the gradients of the i -th chromophore

concentration is obtained by differentiating the objective function given by (2) with respect to the corresponding chromophore concentration as

$$\frac{\partial \phi[C_i]}{\partial C_i} = \sum_{n=1}^{N_\lambda} \sum_{d=1}^{ND} \|M_d^{\lambda_n} - P_d^{\lambda_n}\| \left[-\frac{\partial P_d^{\lambda_n}}{\partial C_i} \right] = \sum_{n=1}^{N_\lambda} \sum_{d=1}^{ND} \|M_d^{\lambda_n} - P_d^{\lambda_n}\| \left[-\epsilon_i^{\lambda_n} \frac{\partial \mu_a^{\lambda_n}}{\partial C_i} \frac{\partial P_d^{\lambda_n}}{\partial \mu_a^{\lambda_n}} \right] \quad (3)$$

where $\partial P_d^{\lambda_n} / \partial C_i$ denotes the gradient of the spectral measurement $P_d^{\lambda_n}$ with respect to i -th chromophore concentration. Once we obtain the gradients with respect to all chromophore concentrations, we search for the descent direction and then iteratively make corrections to the unknowns. In our case all these calculations are performed with the limited memory version of the BFGS method [10].

3. Results: Numerical simulations and small animal imaging

We have performed extensive numerical studies to test and characterize the performance of the code. As an example, we show here results that illustrate the importance of choosing appropriate wavelength pairs for optimal reconstruction results. To mimic small-animal-imaging geometries, we consider a 2cm-in-diameter cylinder. This cylinder contains two smaller areas with varying oxy-hemoglobin [HbO₂] and deoxy-hemoglobin [Hb] concentrations. In one area [HbO₂] is set to 40 μ M and in the other area [Hb] = 20 μ M. For the background medium we chose [HbO₂] = 20 μ M and the [Hb] = 10 μ M. Here we consider two different wavelength sets, ($\lambda_1 = 650$ nm, $\lambda_2 = 866$ nm) and ($\lambda_1 = 780$ nm, $\lambda_2 = 866$ nm). For both set the molar extinction coefficients of HbO₂ and Hb are clearly distinguished from each other.

To quantify the accuracy of the reconstructed image, we use two metrics, a correlation coefficient ρ_c and a deviations factor ρ_d . The larger ρ_c (closer to 1) and the smaller ρ_d (closer to zero), the better the image reconstruction result. Figure 1 shows the images of [HbO₂] and [Hb] obtained from these different wavelength sets. The corresponding correlation coefficients and deviation factors are given in Table 1. As can be seen, the (650nm, 866nm) set gives more accurate results. This wavelength set results in larger ρ_c values and smaller ρ_d values for both [Hb] and [HbO₂] images. as compared to the results for the (780nm, 866nm) wavelength pair. The (780nm, 866nm) set shows a strong crosstalk between [Hb] and [HbO₂] reconstructions. This poor performance may be explained by the concept of a condition number $\kappa(E)$ of the extinction coefficient matrix E that represents a measure of how ‘well-posed’ a problem is; the larger $\kappa(E)$ is, the more ‘ill-posed’ is the system. In our case, the condition numbers for the (650 nm, 866nm) and (780nm, 866nm) sets are 1.7 and 4.6 respectively.

In addition to numerical studies we have started to explore the code performance in experiments involving bearing mice. An example is shown in Fig. 2. The data was acquired with a dynamic near-infrared optical tomographic (DYNOT) system that has two sources that emit light in a steady-state mode at $\lambda = 760$ and $\lambda = 830$ nm. The animal, in whose kidney a Willms tumor had been growing for 40 days, is placed in a 5-cm-diameter cylinder that is surrounded by two fiber-holding rings, which are in contact with the surface of the cylinder. Each ring has 12 sources and 12 detectors spaced at 15° intervals. The cylinder partially filled with a 1% intralipid fluid serves to reduce the edge effects during the reconstruction. More detailed information about the animal model and DYNOT system can be found elsewhere [11, 12].

Since our instrument does not provide the absolute measurements due to the unknown calibration errors such as photon loss in fibers, we employed the following objective function [13]:

$$\phi[\text{HbO}_2, \text{HbR}] = \frac{1}{2} \sum_{\lambda} \sum_s \sum_d \left\| \frac{M_{\text{tar},s,d}^{\lambda} P_{\text{ref},s,d}^{\lambda} - P_{\text{tar},s,d}^{\lambda}}{M_{\text{ref},s,d}^{\lambda}} \right\|^2 \quad (4)$$

where the subscripts s and d denote the numbers of sources and detectors. $M_{\text{tar},s,d}^{\lambda}$ and $M_{\text{ref},s,d}^{\lambda}$ denote the spectral measurements at wavelength λ for the target medium of unknown optical properties and the reference medium of known optical properties, respectively. $P_{\text{ref},s,d}^{\lambda}$ and $P_{\text{tar},s,d}^{\lambda}$ are the corresponding forward predictions for the reference medium of known optical properties and the target medium of unknown optical properties, respectively. Figure 2a shows an example of a time trace of measured optical signals for one source-detector pair. The treatment was

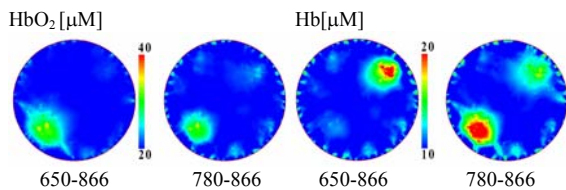


Fig. 1. Images of reconstructed hemoglobin concentrations, HbO₂ and Hb, obtained with the multi-spectral method for two wavelength sets: 650-866nm and 780-866nm.

Table 1. Image quality of reconstructed hemoglobin concentrations obtained with the multi-spectral method for two wavelength sets.

λ set	Error of [HbO ₂]		Error of [Hb]	
	correlation	deviation	correlation	deviation
650-866	0.69	0.72	0.65	0.84
780-866	0.61	0.79	0.23	1.64

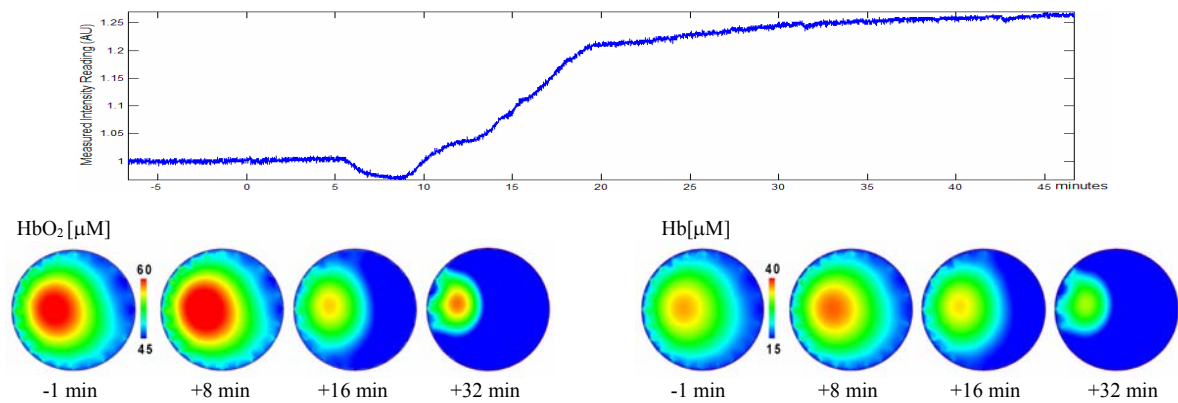


Fig. 2. Time trace images of reconstructed $[\text{HbO}_2]$ and $[\text{Hb}]$ distributions obtained with two wavelengths measurements (760 and 830 nm); (a) measured intensity for an example source detector pair; (b) reconstruction images

administered at time 0 and a signal dip occurs between 6 to 9 minutes after the injection. A steep sustained signal increase begins just after the dip at 9 minutes and remains for the remainders of the experiment, but becomes more gradual after 20 minutes.

The signal decreases and increases in the time trace are believed to be caused by increases and decreases in $[\text{HbO}_2]$ and $[\text{Hb}]$, which influences the light absorption. The characteristic of the time trace's signature is faithfully reflected in the reconstruction results for $[\text{HbO}_2]$ and $[\text{Hb}]$ distributions, as shown in Figure 2b. Compared to the image obtained 1 minute before the drug was administered, we observe an increase of $[\text{HbO}_2]$ and $[\text{Hb}]$ at 8 minutes after treatment. At 16 minutes, the images for $[\text{HbO}_2]$ and $[\text{Hb}]$ show a sharp decrease when compared to images taken at -1 and +8 minutes. This corresponds well with the change in signal magnitude shown in Figure 1a. These results demonstrate that the direct multi-spectral method gives reasonable results consistent with observations. It should also be noted that the transport-theory-based direct method does not produce any negative values in hemoglobin concentrations, which we observed using the two-step method, with the same code.

This work was supported in part by a grant from the National Institute for Biomedical Imaging and Bioengineering (NIBIB-R01-001900). Furthermore, we would like to thank J. Kandel and D. Yamashiro in providing assistance with the animal model.

5. References

- [1] A.H. Hielscher, A.Y. Bluestone, G.S. Abdoulaev, A.D. Klose, J. Lasker, M. Stewart, U. Netz, J. Beuthan, "Near-infrared diffuse optical tomography," *Disease Markers* 18(5-6), pp. 313-337 (2002).
- [2] A. Li, Q. Zhang, J. P. Culver, E. L. Miller, and D. Boas, "Reconstructing chromosphere concentration images directly by continuous-wave diffuse optical tomography," *Opt. Lett.* 29, 256-258 (2004).
- [3] A. Corlu, T. Durduran, R. Choe, M. Schweiger, E. M. C. Hillman, S. R. Arridge, and A. G. Yodh, "Uniqueness and wavelength optimization in continuous-wave multispectral diffuse optical tomography," *Opt. Lett.* 28, 2339-2341 (2003).
- [4] A. Corlu, R. Choe, T. Durduran, K. Lee, M. Schweiger, S. R. Arridge, E. M. C. Hillman, and A. G. Yodh, "Diffuse optical tomography with spectral constraints and wave optimization," *Applied Optics* 44, 2082-2093 (2005).
- [5] A. H. Hielscher, A. E. Alcouffe, and R. L. Barbour, "Comparison of finite-difference transport and diffusion calculations for photon migration in homogeneous and heterogeneous tissues," *Phys. Med. Biol.* 43, 1285-1302 (1998).
- [6] K. Ren and A. Hielscher, "Frequency domain optical tomography based on the equation of radiative transfer," *SIAM J. Sci. Comp.*, 28, 1463-89(2006).
- [7] H. K. Kim and A. Charette, "A sensitivity function-based conjugate gradient method for optical tomography with the frequency-domain equation of radiative transfer," *J. Quant. Spec. Rad. Trans.* 104, 24-39(2007).
- [8] Y. Saad, "GMRES: A generalized minimum residual algorithm for solving nonsymmetric linear systems," *SIAM Journal of Scientific and Statistical Computing* 7, 856-869(1986).
- [9] S. Prahl, "Optical properties spectra", retrieved 16 March 2003, <http://omlc.ogi.edu/spectra/index.html>, 2001.
- [10] J. Nocedal and S. J. Wright, *Numerical optimization*, Springer-Verlag, New York, 1999.
- [11] J. Masciotti, F. Provenzano, J. Papa, A. Klose, J. Hur, X. Gu, D. Yamashiro M.D., J. Kandel M.D., A. H. Hielscher, "Monitoring tumor growth and treatment in small animals with magnetic resonance optical tomographic imaging," in *Multimodal Biomedical Imaging*, Fred S. Azar, Dimitris N. Metaxas, eds., SPIE International Symposium on Biomedical Optics, Proc. SPIE 6081, #608105 (2006).
- [12] C.H. Schmitz, M. Löcker, J.M. Lasker, A.H. Hielscher, R.L. Barbour, "Instrumentation for fast functional optical tomography," *Rev. of Scientific Instruments* 73(2), pp. 429-439 (2002).
- [13] A. Y. Bluestone, M. Stewart, B. Lei, I. S. Kass, J. Lasker, G. S. Abdoulaev and A. H. Hielscher, "Three-dimensional optical tomographic brain imaging in small animals, Part I: Hypercapnia," *Journal of Biomedical Optics* 9, 1046-1062(2004).